Non-conventional captive manoeuvring tests

Katrien Eloot[1], Marc Vantorre[1],[2]
[1] Ghent University, Technologiepark Zwijnaarde 9, B9052 Gent, Belgium
[2] c/o Flanders Hydraulics, Berchemlei 115, B2140 Antwerpen, Belgium
katrien.eloot@rug.ac.be, marc.vantorre@rug.ac.be, marc.vantorre@lin.vlaanderen.be

Abstract

The introduction of computerised planar motion carriages (CPMC) offered many advantages to researchers making use of captive model testing for investigating ship manoeuvring. Compared to PMM systems of the first generation, a CPMC is restricted to neither small amplitude motions nor captive manoeuvres with harmonic character. Nevertheless it is still not clear in which way optimal use can be made of the possibilities of this experimental equipment in the determination of acceleration derivatives occurring in a ship's mathematical manoeuvring model, especially in shallow water conditions and low speed values. In order to overcome some disadvantages of conventional PMM sway testing, an alternative way of determining sway acceleration derivatives was introduced. A series of captive model tests has been executed using ship models with varying block coefficients – among which a model of the Esso Osaka *– to examine the influence of test parameters on the acceleration derivatives of lateral force and yawing moment during pure sway and yaw motions.*

1. Introduction

The introduction in the early 1960s of the Planar Motion Mechanism allowed the determination of sway acceleration and yaw dependent forces and moments in a relatively narrow tank. Due to mechanical constraints and limitations of available post-processing techniques, PMM systems of the first generation were only able to perform harmonically oscillating sway and yaw motions. Some disadvantages can be recognised: although manoeuvring behaviour is generally considered as a quasi-steady problem, non-stationary effects are introduced due to the experimental techniques; moreover, the applied motions can hardly be considered as realistic.

Thanks to the development of computerised planar motion carriages, the harmonic character of the trajectories implied to the ship models can no longer be considered as a restriction. However, the traditional techniques of performing captive manoeuvring tests with ship models were not fundamentally modified by the introduction of the CPMC.

Non-stationary effects can usually be eliminated from PMM test results by an appropriate selection of the test frequencies, allowing extrapolation to zero frequency. Test results obtained in the towing tank for manoeuvres in shallow water at Flanders Hydraulics (Antwerp, Belgium), however, indicate that difficulties may arise in eliminating non-stationary phenomena in (very) shallow water conditions. Especially the results of PMM sway tests appear to be very sensitive to the test frequency, even at very low frequency.

The paper intends to discuss the results of a captive model test program, which was executed in order to acquire more insight in this problem and to provide an answer to following questions.

- Is the hypothesis of quasi-steadiness justified, or should non-stationary effects be taken into account in the formulation of the mathematical manoeuvring model?
- Are conventional, harmonic PMM sway and yaw tests the most appropriate way of obtaining information about the acceleration induced forces, or can alternative, non-conventional captive manoeuvring tests lead to more acceptable results?

2. Experimental investigation

2.1. Characteristics of the experimental equipment

Captive model tests have been executed in the *Towing Tank for Manoeuvres in Shallow Water (co-operation Flanders Hydraulics – Ghent University)* using two ship models with different block coefficients (see Table 1). The dimensions of the towing tank are 88 x 7 x 0.5 m³, with a useful length of 68 m.

Table 1. Characteristics of tested models

	E518		D518
Ship type	Tanker (*Esso Osaka*)		Container carrier
Condition	EG	EH	DA
L_{pp} (m)	325.0		289.8
B (m)	53.0		40.25
D (m)	34.0		22.8
T (m)	21.79		15.0
C_B	0.83		0.61
scale	1/85		1/75
h/T	1.2	1.5	1.2

2.2. Test program

2.2.1. Conventional PMM tests

Conventional PMM sway and yaw tests without propeller and rudder action have been executed with test parameters summarised in Table 2. The non-dimensional frequency is defined as:

$$\omega' = \frac{\omega L_{pp}}{u} \tag{1}$$

u being the longitudinal component of model speed V.

Table 2. Test parameters during conventional PMM tests

	PMM sway tests		PMM yaw tests	
Condition	EG/EH	DA	EG/EH	DA
Froude number F_n (-)	0.033 0.049 0.065	0.032 0.049 0.065	0.016 0.033 0.049 0.065	0.032 0.049 0.065
Frequency range ω' (-)	1 – 6	1 – 4	1.43 – 6.67	2.25 – 4.50
Amplitude y_{0A} (m) ψ_A (deg)	0.25 m 0.50 m 1.00 m	0.25 m 0.50 m 1.00 m	10 deg 15 deg 20 deg 25 deg 35 deg	10 deg 15 deg 20 deg 25 deg 30 deg 35 deg

According to the Froude numbers only lower model velocities have been considered during the test program. The selection of these speed values is justified taking account of the shallow water conditions in which the manoeuvres are carried out, but differ substantially from the speed values used during oscillatory captive model tests reported in many papers concerning PMM testing such as [1] and [2]. Nevertheless, tests carried out in similar conditions were reported in [3] where the influence of water depth and speed on the manoeuvring derivatives has been examined.

2.2.2. Non-conventional PMM tests

Non-conventional PMM sway tests have been introduced to overcome some disadvantages related to traditional sway tests.

- Discontinuities in the sway acceleration are introduced at the beginning and the end of the stationary oscillation phase, described by the formulas:

$$y = y_{0A} \cos \omega t$$
$$v = -v_A \sin \omega t \qquad (2)$$
$$\dot{v} = -\dot{v}_A \cos \omega t$$

- Depending upon the imposed (non-dimensional) oscillation frequency, interference may occur between the trajectories described by the fore and aft body of the model. High frequencies ω' impose interference over a relatively substantial fraction of the oscillation period, as is illustrated in figure 1. As this kind of interference takes place at maximum sway acceleration, the determination of the acceleration derivative may be affected. These so-called 'memory effects' occurring during captive model testing are illustrated in [4] based on a idealised two fin craft.
- The sway acceleration reaches a maximum at zero sway velocity. At low oscillation frequency, this may lead to control inaccuracies, especially in the case of a CPMC with independent control of the three degrees of freedom.
- The motion imposed to the ship model may be considered as rather unrealistic.

These disadvantages are eliminated by the introduction of non-conventional sway tests, first reported in [5], where a constant forward speed is combined with alternating sway motions to starboard (phase I) and port (phase III). Both phases are separated by a so-called link period (phase II), during which the model is kept in its maximum lateral position, allowing the aft body to leave the fore body's 'lateral wake'.

During phases I and III, with duration $\Delta x_0/u_0$, the lateral position is varied as follows:

$$y_0 = y_{0,gem} + (-1)^i \left(\frac{\Delta y_0}{2} - \frac{\Delta y_0}{\Delta x_0} u_0 (t - t'_{i0}) + \frac{\Delta y_0}{2\pi} \sin \omega * (t - t'_{i0}) \right) \qquad (3)$$

During the link period, with duration $\Delta L/u_0$, the lateral position is constant:

$$y_0 = y_{0,gem} + (-1)^i \frac{\Delta y_0}{2} \qquad (4)$$

3. PMM sway tests

The influence of sway acceleration on the lateral force appears to be more important than the influence on yawing moment. More attention will be paid to the derivative Y'_{vdot} in the next chapters.

3.1. Conventional PMM sway tests

The results of captive model tests for the non-dimensional acceleration derivative Y'_{vdot}:

$$Y'_{\dot{v}} \equiv Y'_{vdot} = \frac{Y_{vdot}}{\frac{1}{2}\rho L_{pp}^2 T} \tag{5}$$

are presented on figure 2 for the Esso Osaka model at two water depths, and on figure 3 for the containership D518 at several forward speeds. These values are based on a Fourier analysis (up to the third harmonic) of the lateral forces measured on the fore and aft gauges.

The effect of the underkeel clearance is clearly illustrated in figure 2. As the water depth decreases, the influence of frequency on the acceleration derivative increases considerably. At lower frequency the scatter becomes very important which makes an extrapolation to zero frequency impossible.

This scatter can partly be explained as follows. At low oscillation frequency, the lateral force component due to sway acceleration becomes less important compared to the force component induced by sway velocity. In order to quantify the relative magnitude of the sway acceleration dependent terms, an angle ϕ is defined:

$$\phi = \text{Arc}\tan\left(\frac{Y_s^{[1]}}{Y_c^{[1]}}\right) \tag{6}$$

with $Y_s^{[1]}$ (related to sway velocity) and $Y_c^{[1]}$ (related tot sway acceleration) the first harmonic sine and cosine component obtained by Fourier analysis of the lateral force. If ϕ takes values near ± 90 degrees, only a minor part of the total lateral force is caused by sway acceleration, so that some doubt may arise about the accuracy or the reliability of Y_{vdot}. This can be illustrated applying following formulation for the lateral forces due to sway motion:

$$\begin{aligned} Y &= (Y_{\dot{v}} - m)\dot{v} + Y_{uv}uv + Y_{v|v|}v|v| \\ &= -(Y_{\dot{v}} - m)\omega^2 y_{0A}\cos\omega t - Y_{uv}u\omega y_{0A}\sin\omega t - Y_{v|v|}\omega^2 y_{0A}^2 \sin\omega t|\sin\omega t| \\ &\equiv -(Y_{\dot{v}} - m)\omega^2 y_{0A}\cos\omega t - \left(Y_{uv}u\omega y_{0A} + \frac{8}{3\pi}Y_{v|v|}\omega^2 y_{0A}^2\right)\sin\omega t + \frac{8}{15\pi}Y_{v|v|}\omega^2 y_{0A}^2 \sin 3\omega t + \ldots \end{aligned} \tag{7}$$

yielding following expression for ϕ:

$$\phi = \text{Arc}\tan\frac{Y_{uv}u\omega y_{0A} + \frac{8}{3\pi}Y_{v|v|}\omega^2 y_{0A}^2}{(Y_{\dot{v}} - m)\omega^2 y_{0A}} = \text{Arc}\tan\frac{Y'_{uv}\left(1 + \frac{8}{3\pi}\frac{Y_{v|v|}}{Y_{uv}}\omega'\frac{y_{0A}}{L}\right)}{(Y'_{\dot{v}} - m')\omega'} \tag{8}$$

with

$$Y'_{uv} = \frac{Y_{uv}}{\frac{1}{2}\rho L_{pp} T} \quad ; \quad Y'_{v|v|} = \frac{Y_{v|v|}}{\frac{1}{2}\rho L_{pp} T} \quad ; \quad m' = \frac{m}{\frac{1}{2}\rho L_{pp}^2 T} \tag{9}$$

Based on (7) the acceleration derivative Y_{vdot} is determined:

$$Y_{\dot{v}} \equiv Y_{vdot} = -\frac{Y_c^{[1]}}{\omega^2 y_{0A}} + m \tag{10}$$

Figure 4 shows that smaller absolute values for the acceleration derivative Y'_{vdot} coincide with $\phi \approx 90$ deg, indicating less reliable measurements. Although identical test parameters are applied for the

conditions EG and EH, larger underkeel clearances lead to more reliable derivatives. A comparison between figures 4 and 5 shows that for slender ships the sway acceleration derivative is derived from smaller force components relative to the sway velocity dependent components.

Values for Y'_{vdot} can be selected by introducing an arbitrarily chosen limit for ϕ. The results for the *Esso Osaka* are compared with those of a tanker with comparable dimensions tested at a Froude number of 0.066 and an underkeel clearance of 21% [3] (figure 6). For the conditions EG and EH the results can also be compared to the values obtained by the Japanese MMG group [6] (see Table 3).

The introduction of a limit for ϕ reduces the scatter according to the frequency considerably. It is remarkable that at lower frequency only tests carried out with small sway amplitude are selected: it appears that increasing sway amplitude does not lead to a more reliable determination of the added mass. Nevertheless, this is in accordance with expression (8).

Table 3. Results for the acceleration derivative Y'_{vdot} according to the MMG group.

	Condition EG, h/T = 1.2		Condition EH, h/T = 1.5	
	m_y/m	Y'_{vdot}	m_y/m	Y'_{vdot}
Esso Osaka model length 2.5m	2.723	-0.736	1.641	-0.444
Esso Osaka model length 6m	2.453	-0.663	1.440	-0.389

3.2. Non-conventional PMM sway tests

Non-conventional PMM sway tests have been executed for the conditions EG, EH and DA with a frequency range $\omega^{*'}$ ($= \omega^* L_{pp}/u$) varying between 2 and 16. Tests at higher frequencies are affected by large oscillations of the lateral forces observed during the consecutive link periods (figure 7). At lower frequencies measured lateral forces are smaller and have almost damped out at the end of the link period (figure 8).

The determination of the acceleration derivative Y'_{vdot} is based on a regression analysis according to the mathematical model:

$$Y = (Y_v - m)v + Y^{(\beta)}(u, v) \tag{11}$$

with $Y^{(\beta)}(u,v)$ a tabular model function of the drift angle β.

As the lateral force measured during consecutive sway motions is influenced by the generation of an oscillating flow in the towing tank, it could be useful to consider only the first sway motion from port to starboard to determine the acceleration derivative Y'_{vdot}. A comparison between the values of the acceleration derivative determined in this way and those based on the complete test run is made in figures 9 and 10. The latter also indicate the frequencies at which tank resonance occurs, which is an additional limitation to the execution of PMM tests.
As the oscillation frequency increases, the difference between the Y'_{vdot} values derived from the complete test run and from the first motion becomes more important, which is especially the case for 50% underkeel clearance. At 20% underkeel clearance this tendency is not so clear.

A comparable angle ϕ can be defined for non-conventional PMM sway tests. Following this criterion, the acceleration derivative can be determined more accurately compared to conventional sway tests.

3.3. Comparison between conventional and non-conventional PMM sway tests

On figures 11 to 16 a comparison is made between the acceleration derivatives for lateral force and yawing moment determined from conventional and non-conventional PMM sway tests for the conditions EG, EH and DA.

The derivative Y_{vdot} differ only slightly for the two test types with the same imposed oscillation frequency, especially for fuller bodies. For the container carrier the difference at higher frequency is substantial. For N_{vdot} the influence of the frequency and the scatter decrease considerably for the non-conventional PMM sway tests and for both ship types.

4. PMM yaw tests

PMM yaw tests are performed to determine both yaw acceleration and yaw velocity derivatives. In this paper, however, only yaw acceleration derivatives of both lateral force ($Y_r \equiv Y_{rdot}$) and yawing moment ($N_r \equiv N_{rdot}$) will be discussed.

Unlike the added mass for sway (Y_{vdot}), determining the added moment of inertia, N_{rdot}, does not cause specific problems. Especially in the case of full form ships (figures 17 and 18), the PMM yaw test parameters (oscillation frequency, model speed, yaw amplitude) appear to have a negligible influence on the acceleration derivative N_{rdot}. For slender bodies, on the other hand, the influence is more pronounced (see figure 19); especially the yaw amplitude appears to have a rather significant influence on the test results. In this case, however, the added moment of inertia is much smaller compared to full ships.

Determining the lateral force acceleration derivative is less straightforward, as the yaw amplitude ψ_A has a considerable influence on the acceleration derivative Y_{rdot} (figures 20 to 22).

The variation of the angle ϕ, defined as (6), explains just a part of this parameter dependence (figures 20 and 22). If following simplified mathematical model is used:

$$\begin{aligned} Y &= (Y_r - mx_G)\dot{r} + (Y_{ur} - m)ur + Y_{r|r|}r|r| \\ &= -(Y_r - mx_G)\omega^2\psi_A \cos\omega t - (Y_{ur} - m)u\omega\psi_A \sin\omega t - Y_{r|r|}\omega^2\psi_A^2 \sin\omega t|\sin\omega t| \\ &\approx -(Y_r - mx_G)\omega^2\psi_A \cos\omega t - \left((Y_{ur} - m)u\omega\psi_A + \frac{8}{3\pi}Y_{r|r|}\omega^2\psi_A^2\right)\sin\omega t + \ldots \end{aligned} \tag{12}$$

following expression for ϕ is found:

$$\phi = \text{Arc}\tan\frac{(Y_{ur} - m)u\omega\psi_A + \frac{8}{3\pi}Y_{r|r|}\omega^2\psi_A^2}{(Y_r - mx_G)\omega^2\psi_A} = \text{Arc}\tan\frac{(Y'_{ur} - m')\left(1 + \frac{8}{3\pi}\frac{Y'_{r|r|}}{Y'_{ur} - m'}\omega'\psi_A\right)}{(Y'_r - m'x'_G)\omega'} \tag{13}$$

As the yaw amplitude increases, the acceleration derivative is determined with more accuracy, as – contrary to the sway induced lateral force – the numerator in (13) decreases, so that yaw acceleration dependent terms become relatively more important. At least, this is the case if $Y'_{r|r|} / (Y'_{ur}-m') < 0$. From this point of view, large amplitude and/or higher frequency yawing tests yield more reliable results. In the case of the Esso Osaka (figures 20-21), some convergence can indeed be noticed if frequency is increased – except for very large amplitude motions – but this is not the case for the container carrier model D (figure 22).

The strong dependence of Y_{rdot} on both frequency and yaw amplitude can qualitatively be explained by interference between the fore and aft body of the ship model occurring during yawing tests. The trajectories followed by the ship model generate complex flow patterns, which may affect the lateral force, and which appear to depend substantially on yaw amplitude, as illustrated in figures 23-24.

At larger underkeel clearances the scatter in Y_{rdot} according to the yaw amplitude becomes smaller, so that the observed problems are related to the water depth to draught ratio.

For the *Esso Osaka* model, the results can be compared to those reported in [6] and [7] (see Table 4).

Table 4. Results for the acceleration derivative Y'_{rdot} and N'_{rdot} according to [6] and [7].

	Condition EG, h/T = 1.2			Condition EH, h/T = 1.5		
	J_{zz}/I_{zz}	N'_{rdot}	Y'_{rdot}	J_{zz}/I_{zz}	N'_{rdot}	Y'_{rdot}
Esso Osaka model L = 2.5 m [6]	1.440	-0.0235		1.138	-0.0186	
Esso Osaka model L = 6.0 m [6]	1.388	-0.0227		1.053	-0.0172	
Esso Osaka model L = 8.125m [7]		-0.0194	-0.0224		-0.0135	-0.0194

Note: Values published in [7] are based on tests carried out with a 1/40 scale model of the *Esso Osaka* at a non-dimensional frequency $\omega' = 5.23$. In [6], only values for N_{rdot} are published.

5. Conclusions

5.1. PMM sway tests

Conventional harmonic PMM sway tests are principally not really suitable for accurate low frequency tests, due to the order of magnitude of the sway acceleration dependent force component relative to the sway velocity dependent force component. Moreover, control inaccuracies may affect the imposed maximum acceleration, especially at low frequency. From this point of view, conventional PMM sway tests appear to give more reliable results at higher frequency and/or small amplitude – for which large amplitude planar motion mechanisms are not required.

On the other hand, motions induced during conventional PMM sway tests cannot be considered as very realistic, due to important interference between the trajectories described by the fore and aft body of the ship model. Only for course-keeping, some exception could be made, as in these conditions oscillations could occur with small amplitude and very low frequency.

During harbour manoeuvring conditions, ship trajectories are more comparable with motions induced during non-conventional PMM sway tests. Berthing manoeuvres with tug assistance, for instance, involve motions with large amplitudes, low frequencies and slow speed, without oscillatory character. Therefore, the motions induced during this alternative type of model testing could be considered to be more realistic. However, this kind of test appears to be very sensitive to tank oscillations.

The water depth appears to be an important parameter: less interpretation problems occur in deep(er) water. Especially in (very) shallow water, the influence of the frequency remains, so that a modified, non-stationary mathematical model is required to take this phenomenon into account during simulations.

5.2. PMM yaw tests

The yaw acceleration derivative of the yawing moment, N'_{rdot}, appears to be not very sensitive to the test parameters, and can be derived with satisfactory accuracy.

The yaw acceleration derivative of the lateral force, Y'_{rdot}, on the other hand, strongly depends on test frequency and, especially, yaw amplitude. These can be explained by the complex flow patterns induced during PMM yaw tests. It is not clear how test parameters should be selected in order to determine realistic values for Y'_{rdot} for a mathematical manoeuvring model, as the realism of the imposed captive manoeuvres depends on the application. For course keeping, small amplitude

motions are more realistic, while in harbour manoeuvres, it may be more appropriate to make use of results of large amplitude motions.

There are indications that conventional PMM yaw tests give more reliable results at high yaw amplitude. From this point of view, the availability of a large amplitude PMM is required.

5.3. General concluding remarks.

Frequency dependence appears to affect the test results derived from (both conventional and non-conventional) PMM tests. These effects can only be incorporated into the mathematical model of a ship manoeuvring simulator if a non-stationary kind of model is implemented.

Some of the PMM test results appear to depend on motion amplitude, which is problematic to incorporate into a mathematical manoeuvring model. There are indications that the use of large amplitude motions does not automatically lead to more realistic or more reliable results.

Most of these effects decrease substantially with increasing water depth. In (relatively) deep water, less interpretation problems occur, and a quasi-stationary approach may be satisfactory.

References

[1] BAILEY, P.A., HUDSON, D.A., PRICE, W.G., TEMAREL, P. (1998), *Theoretical and experimental techniques for predicting seakeeping and manoeuvring ship* characteristics, International Conference on Ship Motions and Manoeuvrability, Paper No. 5, published by RINA, pp. 1-11.

[2] GILL, A.D., PRICE, W.G. (1977), *Determination of the manoeuvring derivatives of a ship model using a horizontal planar motion mechanism in a circulating water channel*, Transactions of the RINA, Vol. 119, pp.161-176.

[3] GILL, A.D., PRICE, W.G. (1978), *Experimental evaluation of the effects of water depth and speed on the manoeuvring derivatives of ship models*, Transactions of the RINA, Vol. 120, pp. 149 - 160.

[4] BISHOP, R.E.D., BURCHER, R.K., PRICE, W.G. (1975), *The determination of ship manoeuvring characteristics from model tests*, Transactions of the RINA, Vol. 117, pp. 215-231.

[5] VANTORRE, M., ELOOT, K. (1997), *Requirements for standard harmonic captive manoeuvring tests*, 4th IFAC Conference on Manoeuvring and Control of Marine Craft, Brijuni, Croatia, pp. 93-98.

[6] Research Committee of Dynamic Performance, Manoeuvring and Control Section (1985), *Prediction of the manoeuvrability of a ship*, Bulletin of the Society of Naval Architects of Japan, No. 668.

[7] BOGDANOV, P., VASSILEV, P., LEFTEROVA, M., MILANOV, E. (1987), *"Esso Osaka" Tanker manoeuvrability investigations in deep and shallow water, using PMM*, International Shipbuilding Progress, Vol.34, No. 390, pp.30-39.

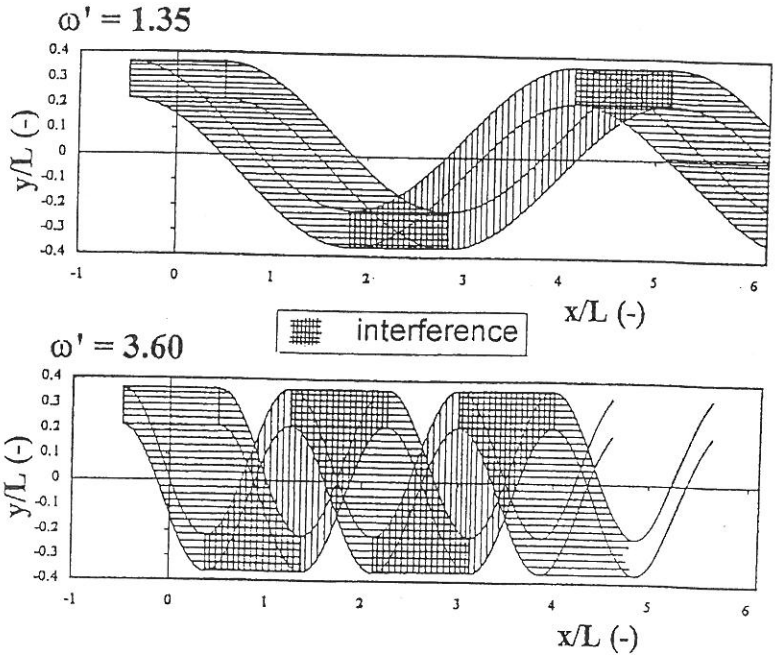

Figure 1. Swept path during harmonic PMM sway tests: influence of non-dimensional frequency.

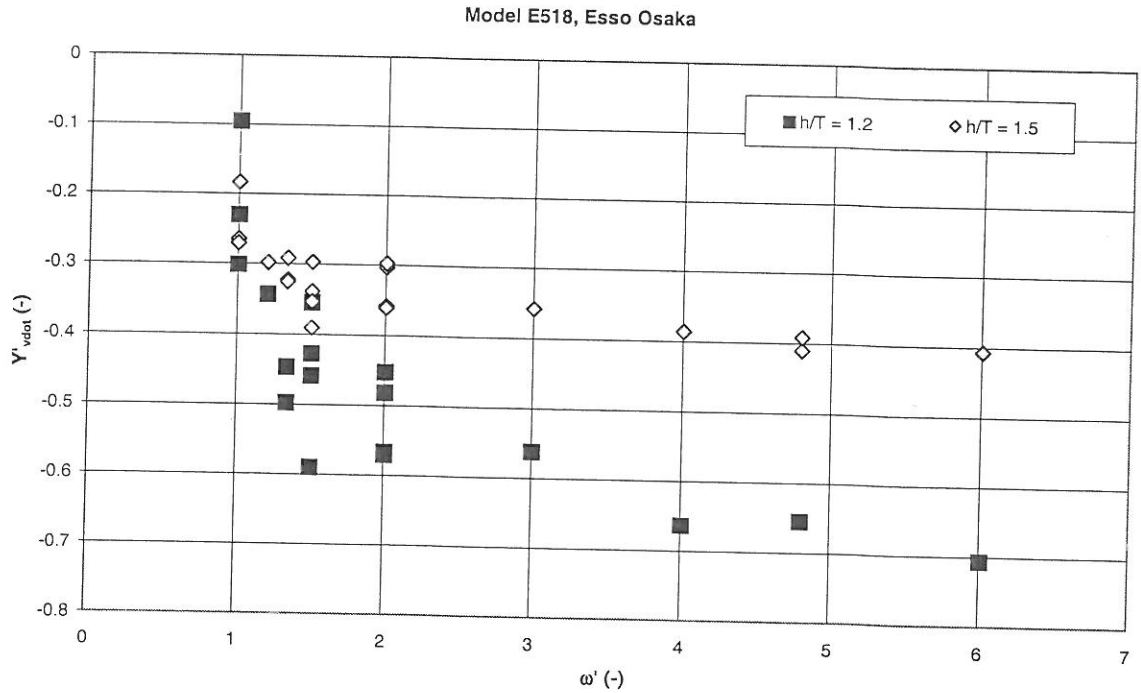

Figure 2. Model E (*Esso Osaka*). Sway acceleration derivative of lateral force, derived from harmonic PMM sway tests.

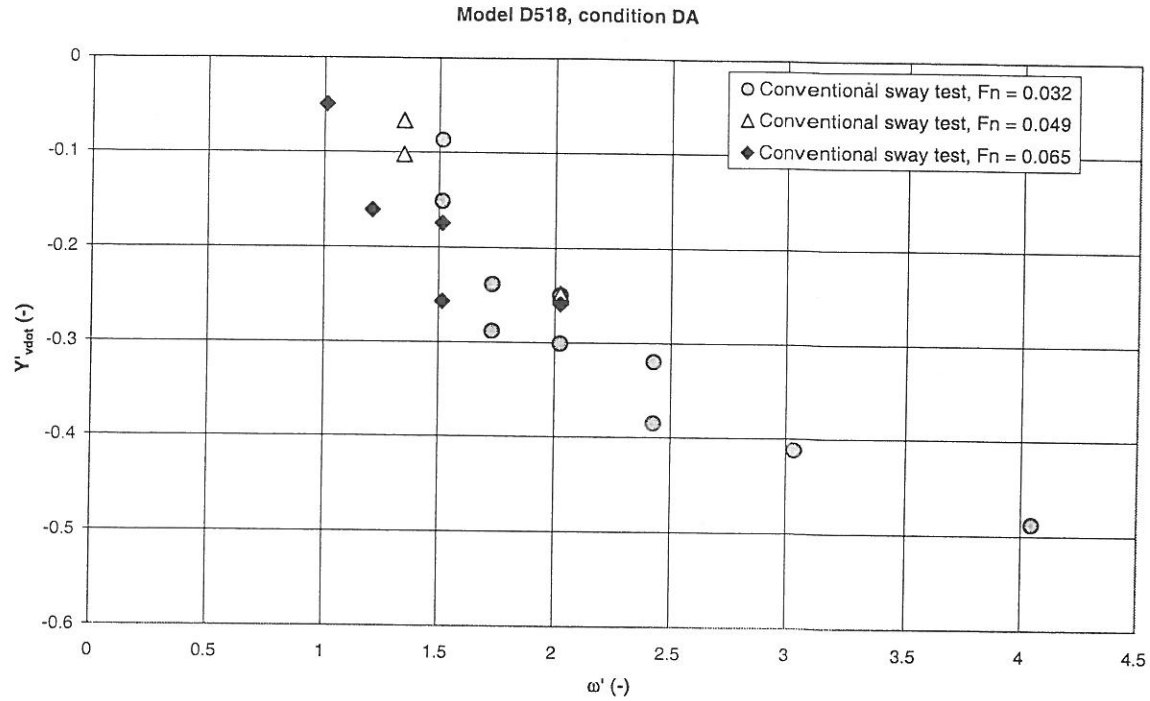

Figure 3. Model D (container carrier). Sway acceleration derivative of lateral force, derived from harmonic PMM sway tests.

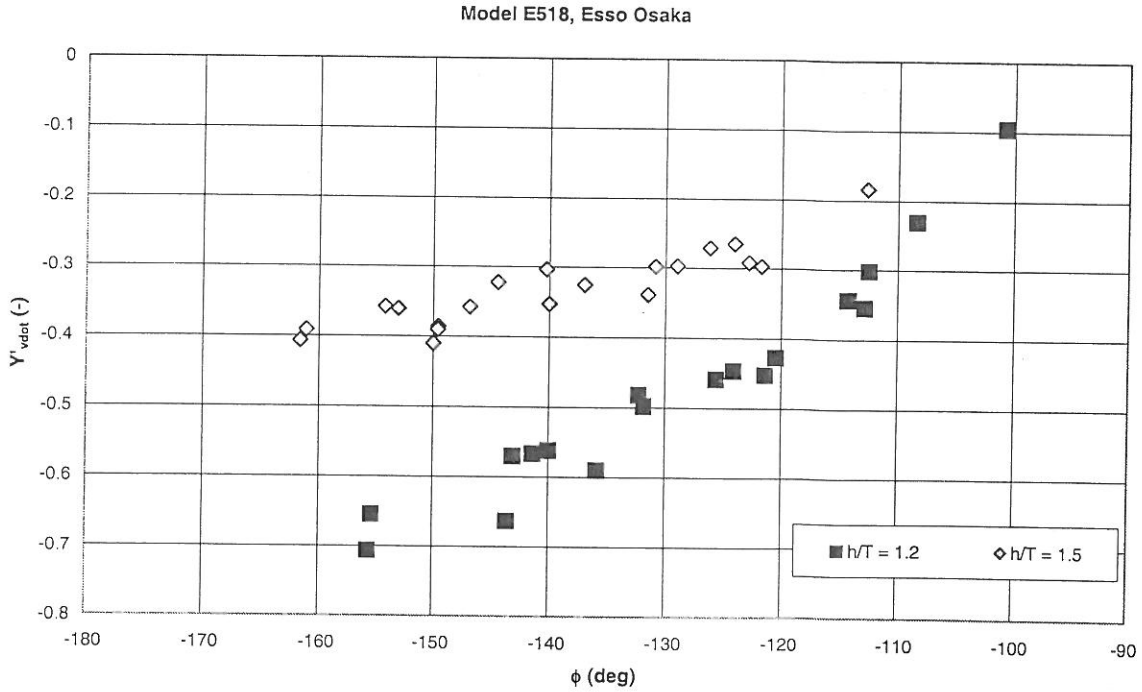

Figure 4. Model E (Esso Osaka). Sway acceleration derivative of lateral force versus phase angle ϕ of force signal.

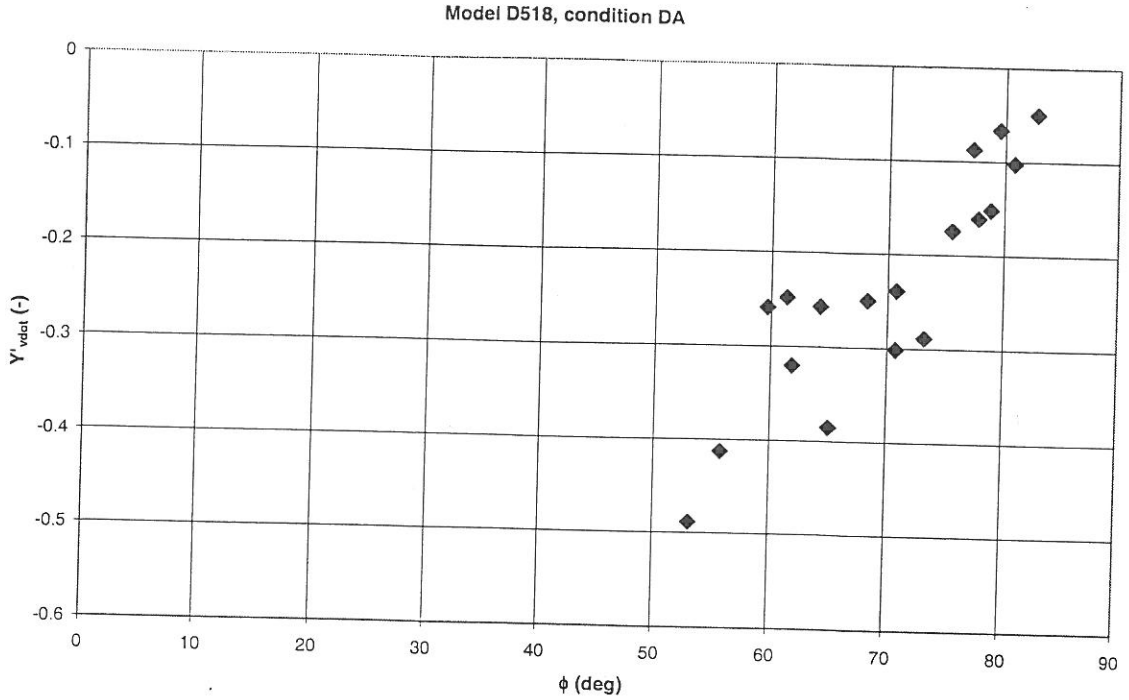

Figure 5. Model D (container carrier). Sway acceleration derivative of lateral force versus phase angle ϕ of force signal.

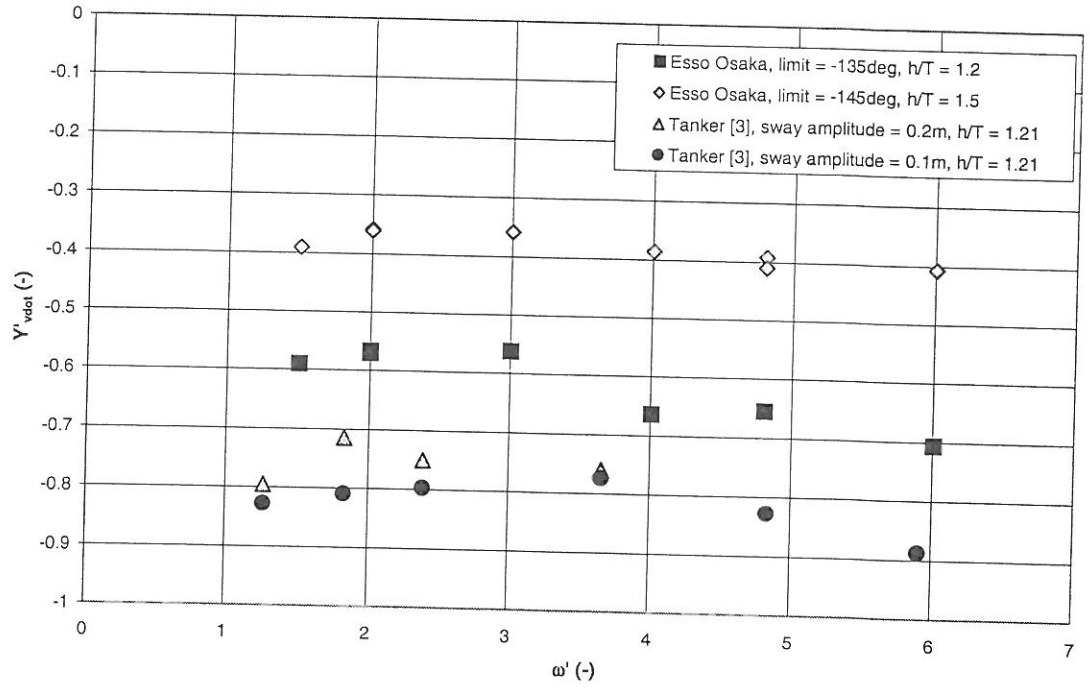

Figure 6. Model E (*Esso Osaka*). Sway acceleration derivative of lateral force vs. non-dimensional frequency. Harmonic PMM sway tests selected by lateral force phase angle; comparison with other published data.

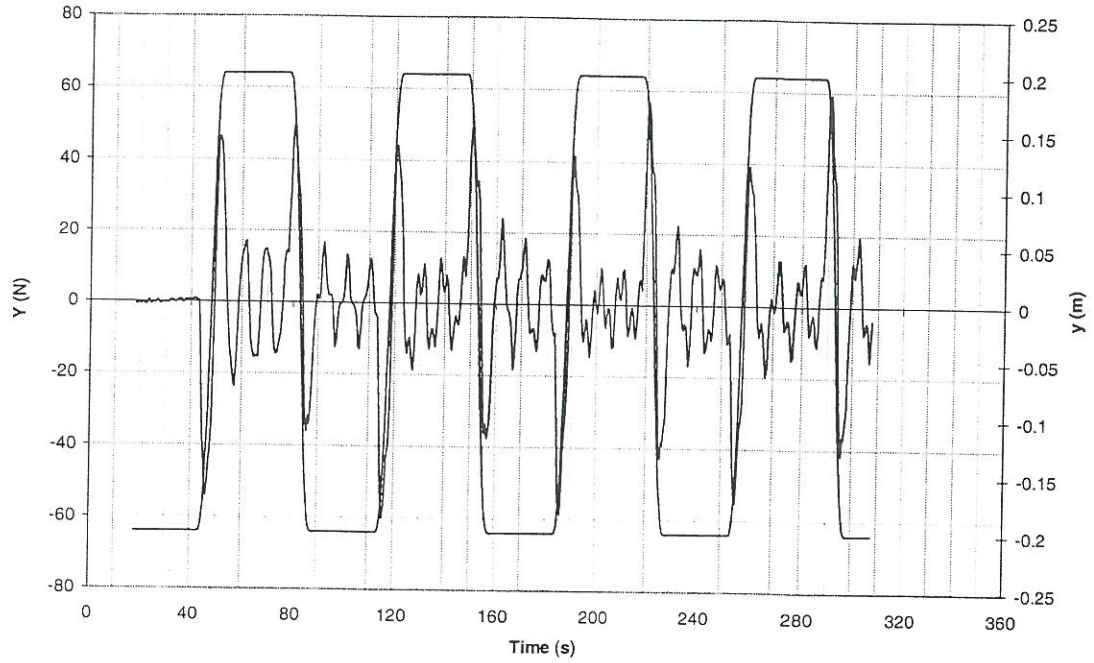

Figure 7. Model E (*Esso Osaka*). Non-conventional PMM sway test (h/T = 1.2, F_n = 0.033, $\omega^{*'}$ = 12): time history of lateral force.

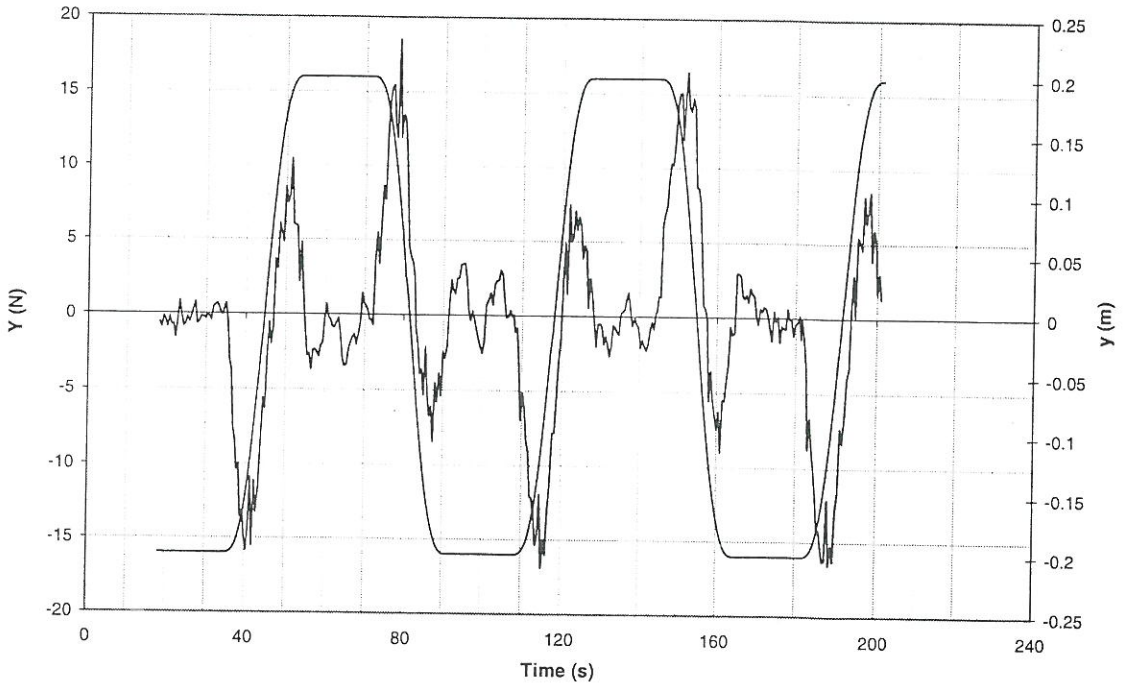

Figure 8. Model E (*Esso Osaka*). Non-conventional PMM sway test (h/T = 1.2, F_n = 0.049, $\omega^{*'}$ = 6): time history of lateral force.

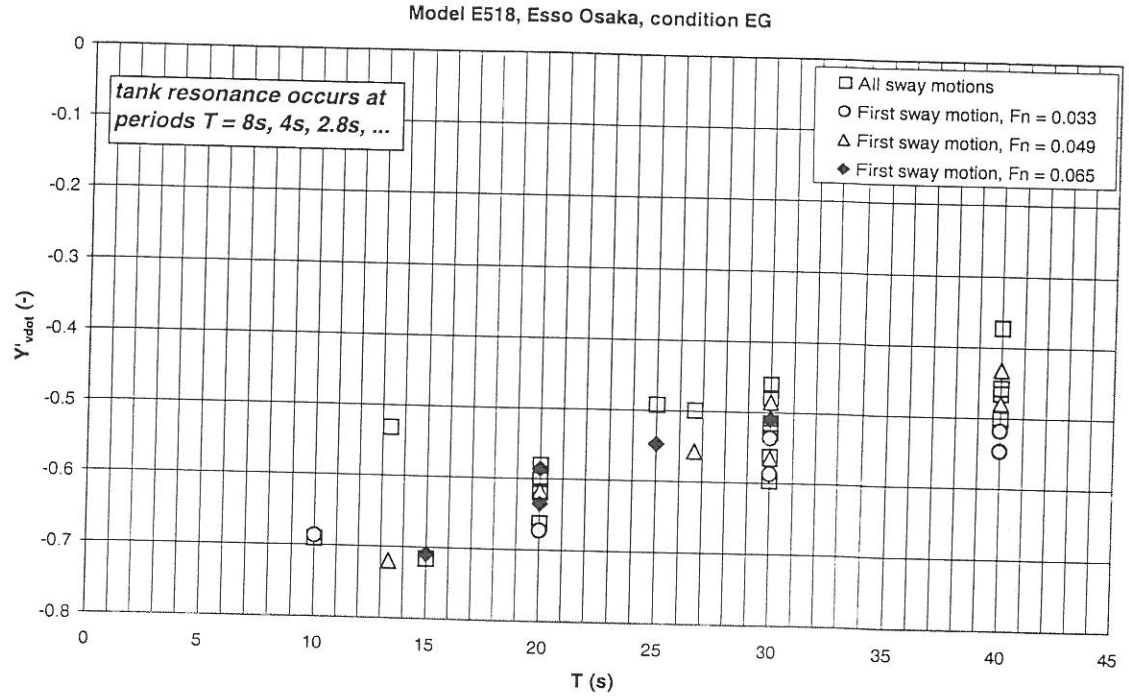

Figure 9. Model E (*Esso Osaka*), h/T = 1.2. Results of non-conventional PMM sway tests: sway acceleration derivative of lateral force vs. period T (= $2\pi/\omega^*$).

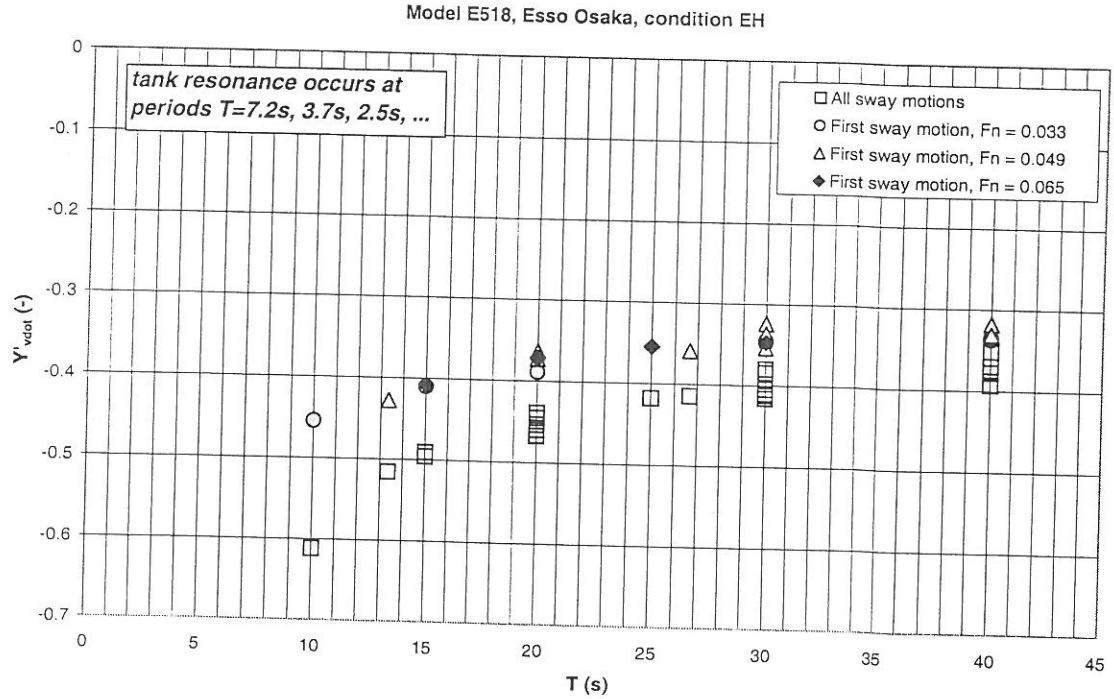

Figure 10. Model E (*Esso Osaka*), h/T = 1.5. Results of non-conventional PMM sway tests: sway acceleration derivative of lateral force vs. period T (= $2\pi/\omega^*$).

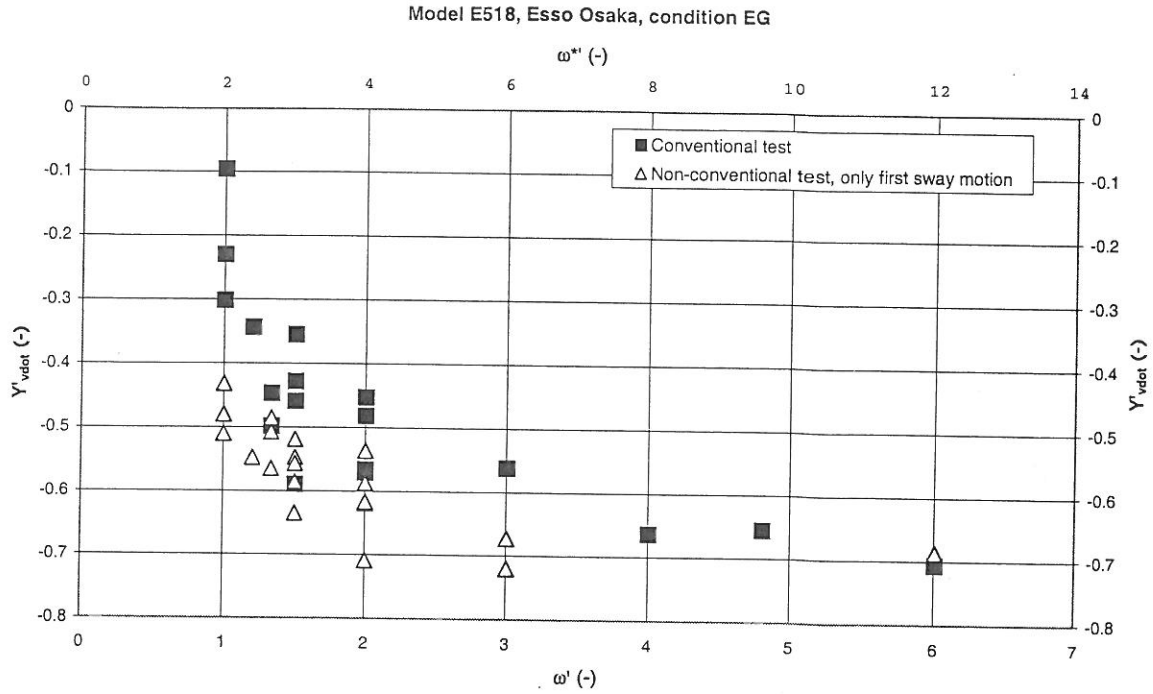

Figure 11. Model E (*Esso Osaka*), h/T = 1.2. Sway acceleration derivative of lateral force, derived from harmonic and non-conventional PMM sway tests as a function of test frequency.

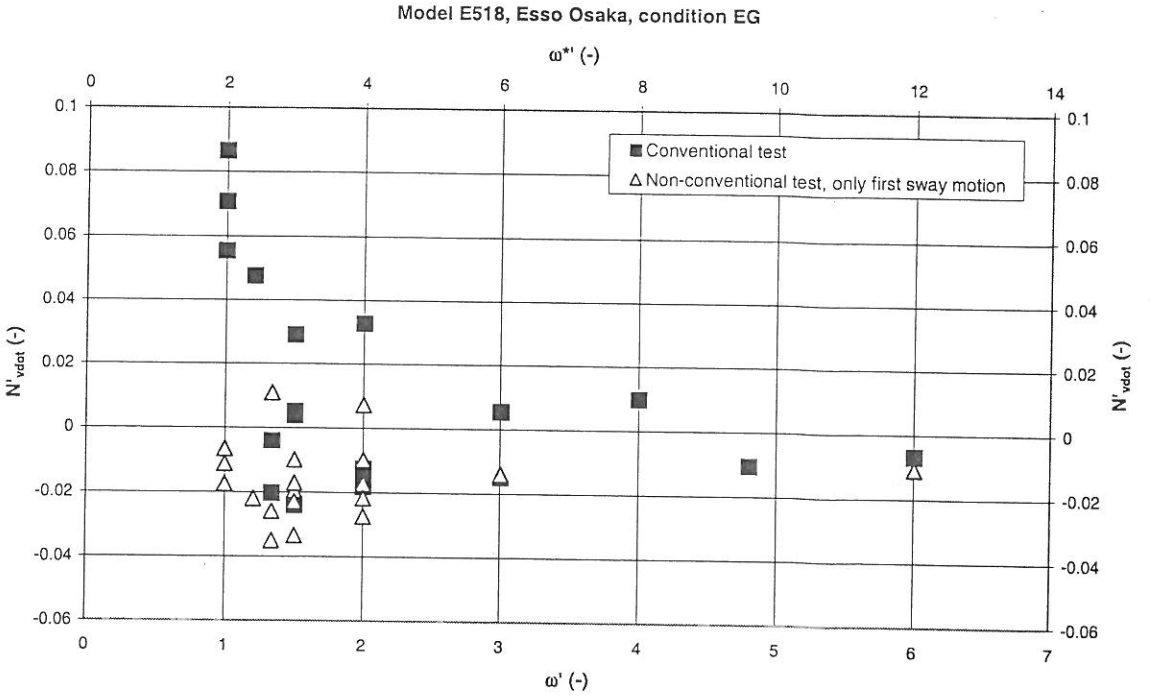

Figure 12. Model E (*Esso Osaka*), h/T = 1.2. Sway acceleration derivative of yawing moment, derived from harmonic and non-conventional PMM sway tests as a function of test frequency.

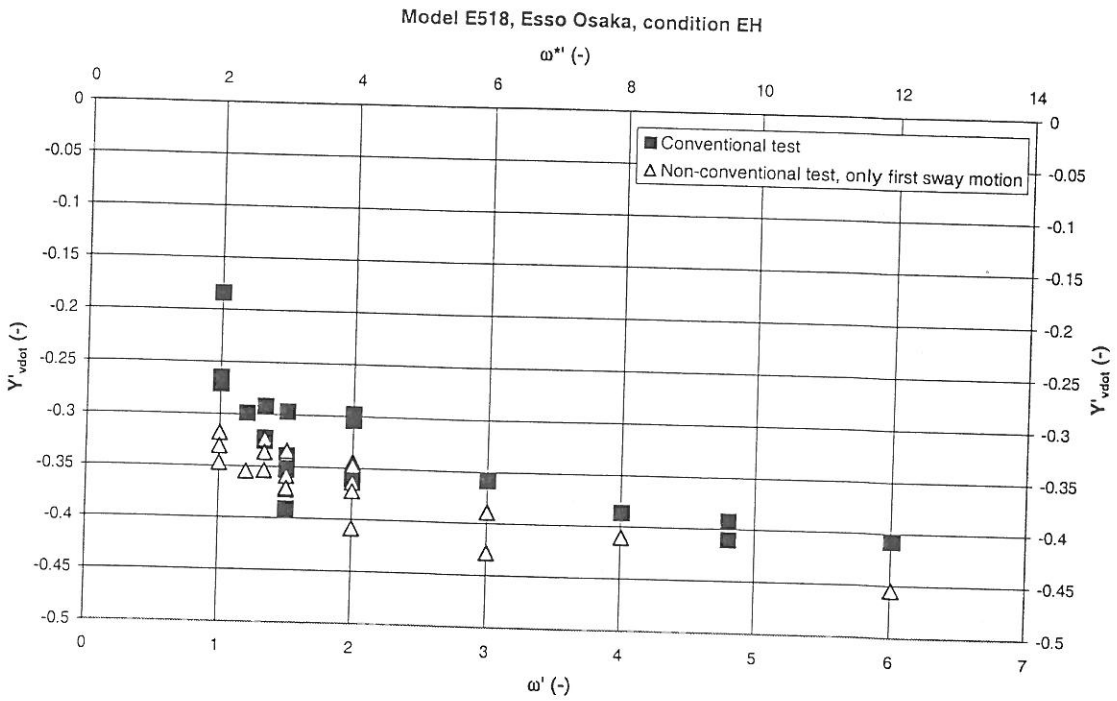

Figure 13. Model E (*Esso Osaka*), h/T = 1.5. Sway acceleration derivative of lateral force, derived from harmonic and non-conventional PMM sway tests as a function of test frequency.

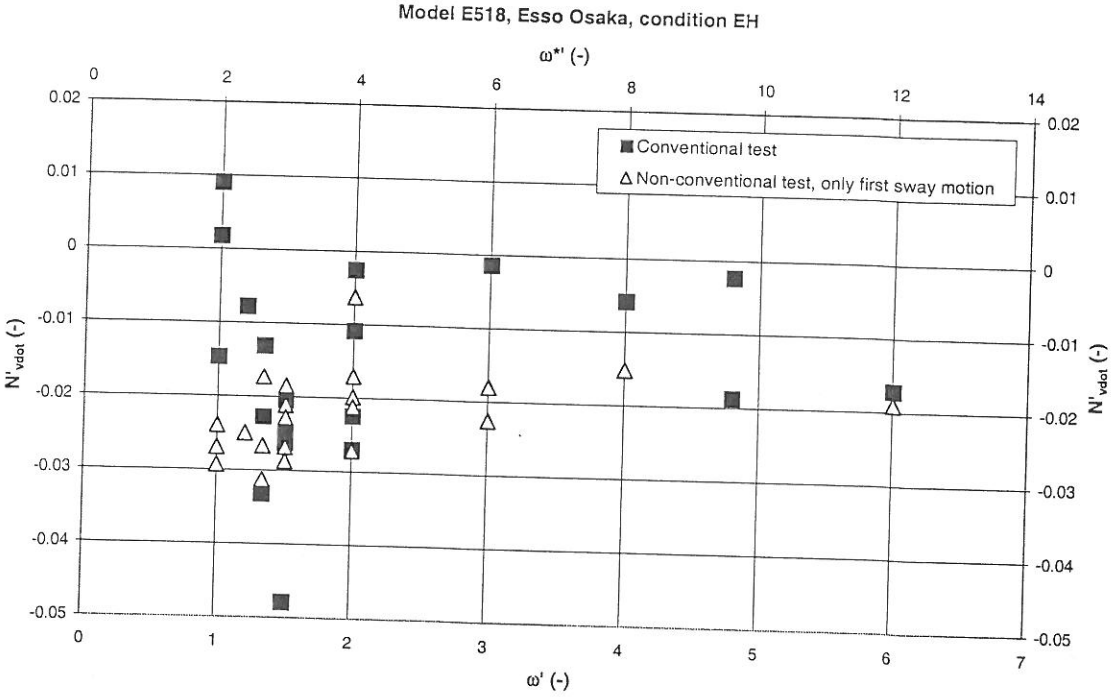

Figure 14. Model E (*Esso Osaka*), h/T = 1.5. Sway acceleration derivative of yawing moment, derived from harmonic and non-conventional PMM sway tests as a function of test frequency.

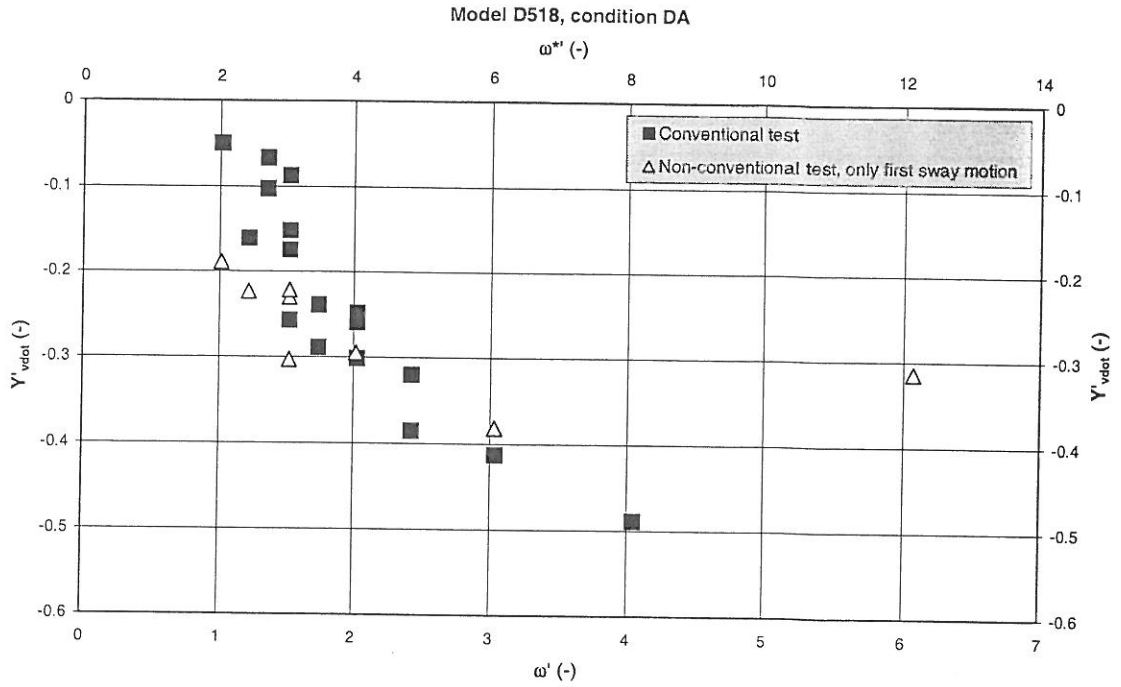

Figure 15. Model D (container carrier), h/T = 1.2. Sway acceleration derivative of lateral force, derived from harmonic and non-conventional PMM sway tests as a function of test frequency.

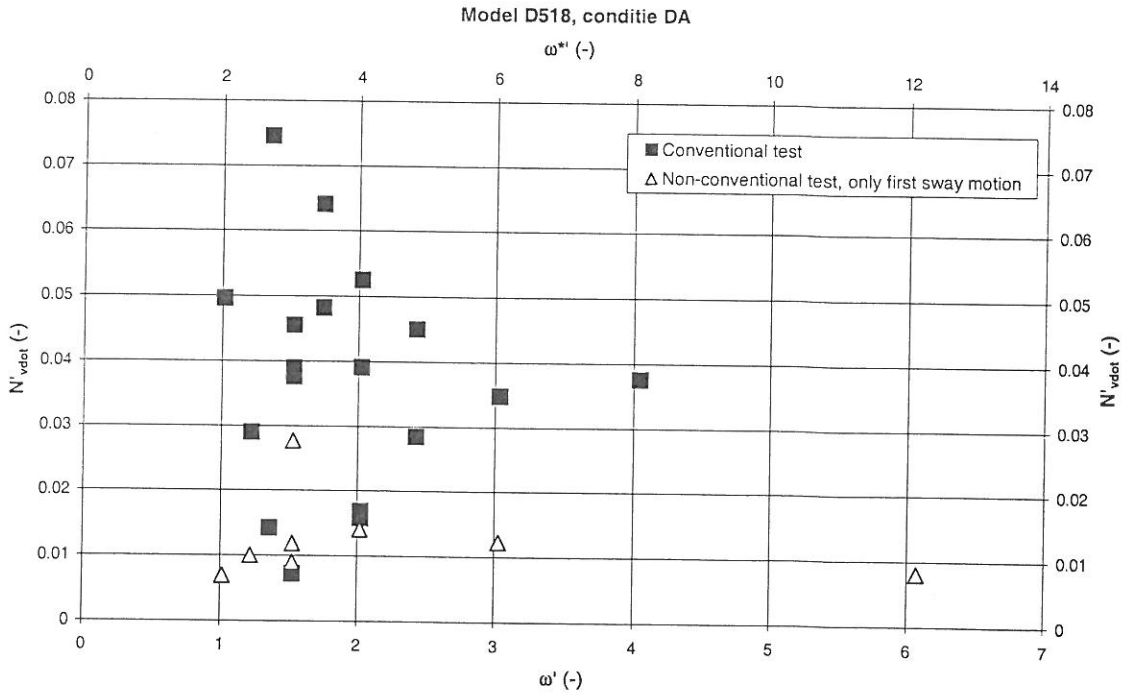

Figure 16. Model D (container carrier), h/T = 1.2. Sway acceleration derivative of yawing moment, derived from harmonic and non-conventional PMM sway tests as a function of test frequency.

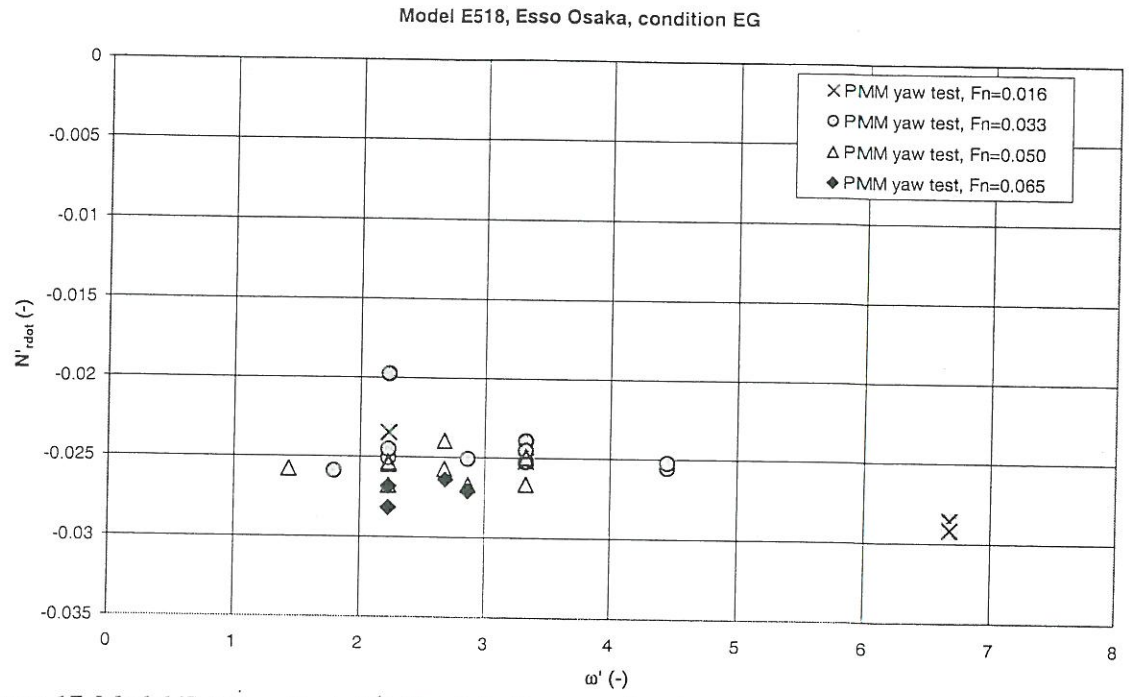

Figure 17. Model E (*Esso Osaka*), h/T = 1.2. Yaw acceleration derivative of yawing moment, derived from PMM yaw tests, as a function of test frequency.

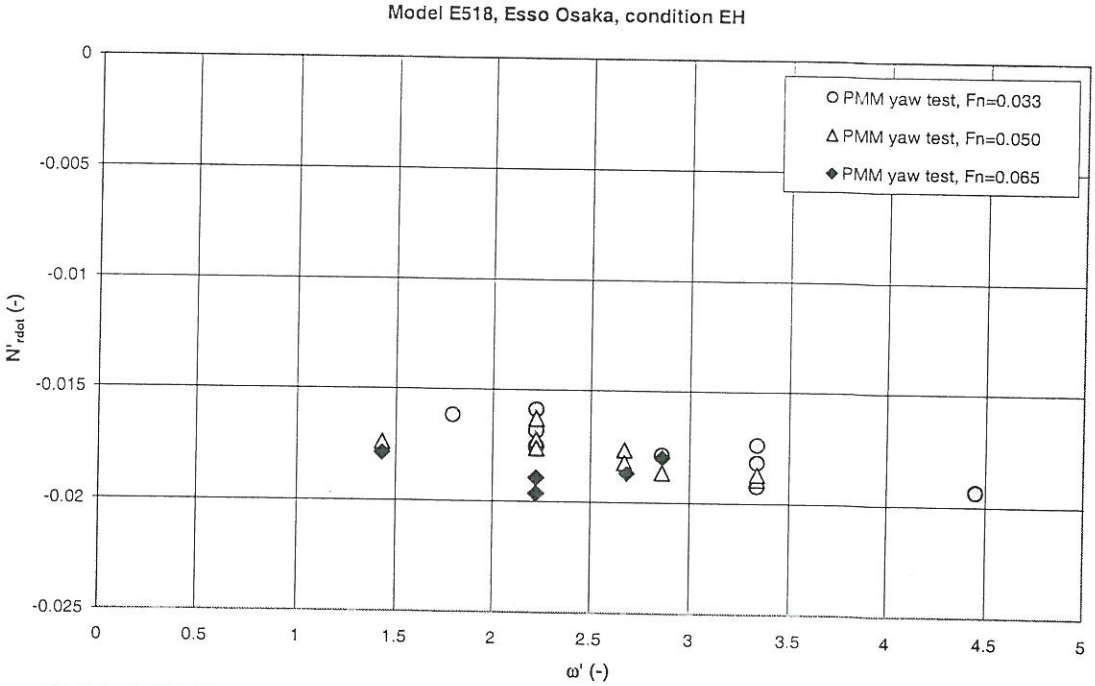

Figure 18. Model E (*Esso Osaka*), h/T = 1.5. Yaw acceleration derivative of yawing moment, derived from PMM yaw tests, as a function of test frequency.

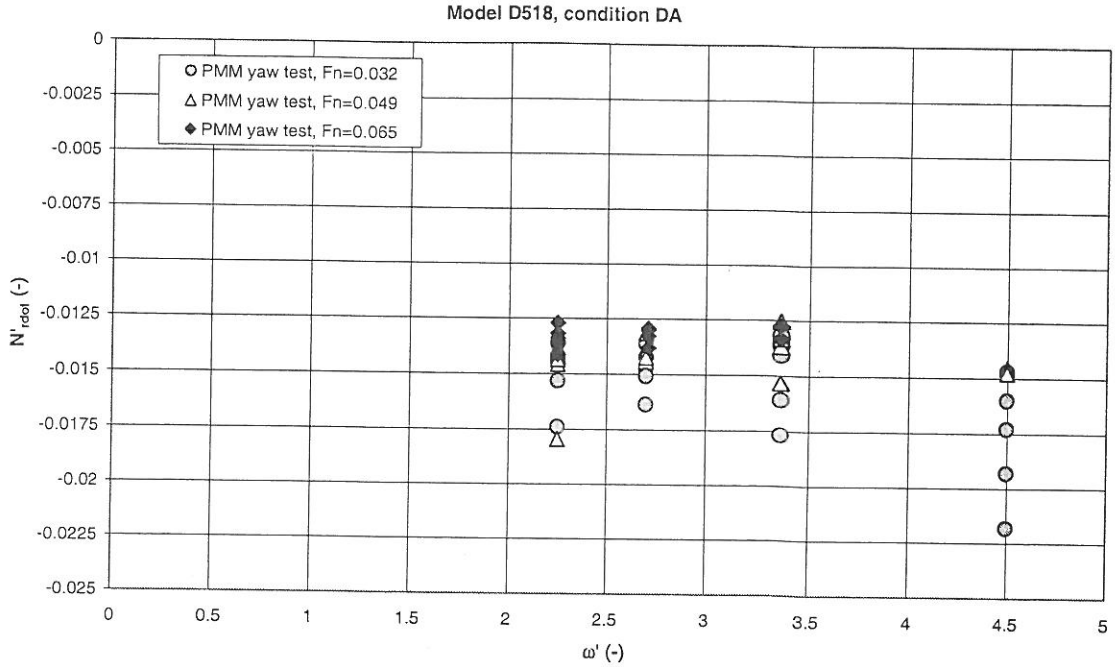

Figure 19. Model D (container carrier), h/T = 1.2. Yaw acceleration derivative of yawing moment, derived from PMM yaw tests, as a function of test frequency.

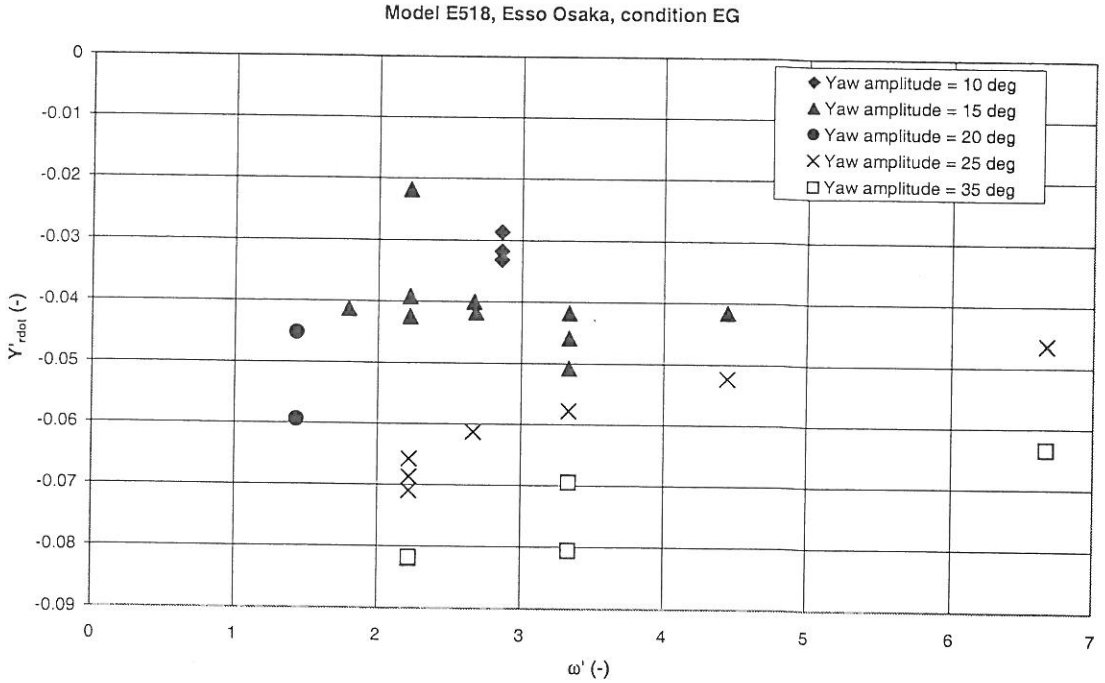

Figure 20. Model E (Esso Osaka), h/T = 1.2. Yaw acceleration derivative of lateral force, derived from PMM yaw tests, as a function of test frequency.

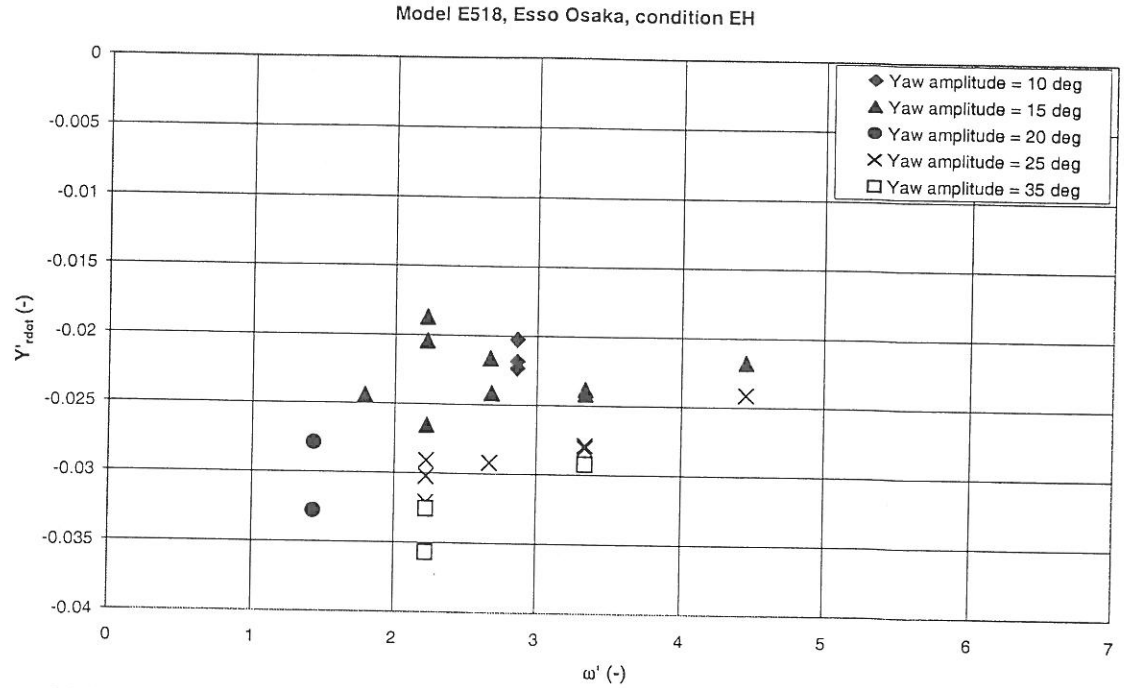

Figure 21. Model E (Esso Osaka), h/T = 1.5. Yaw acceleration derivative of lateral force, derived from PMM yaw tests, as a function of test frequency.

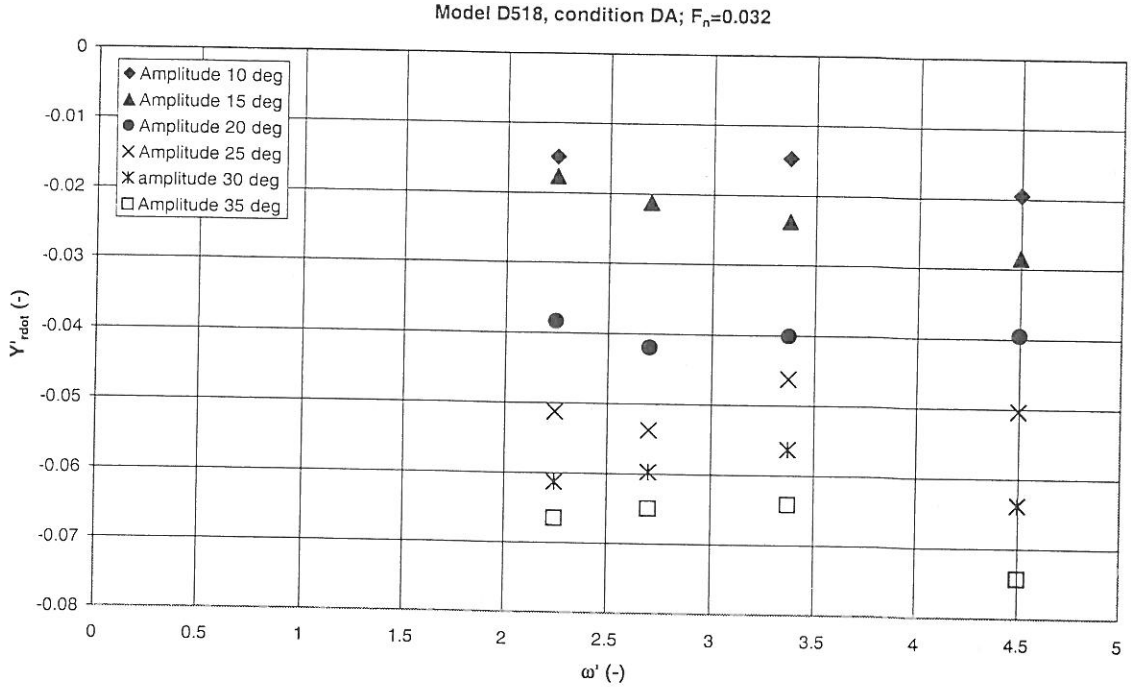

Figure 22. Model D (container carrier), h/T = 1.2. Yaw acceleration derivative of lateral force, derived from PMM yaw tests, as a function of test frequency.

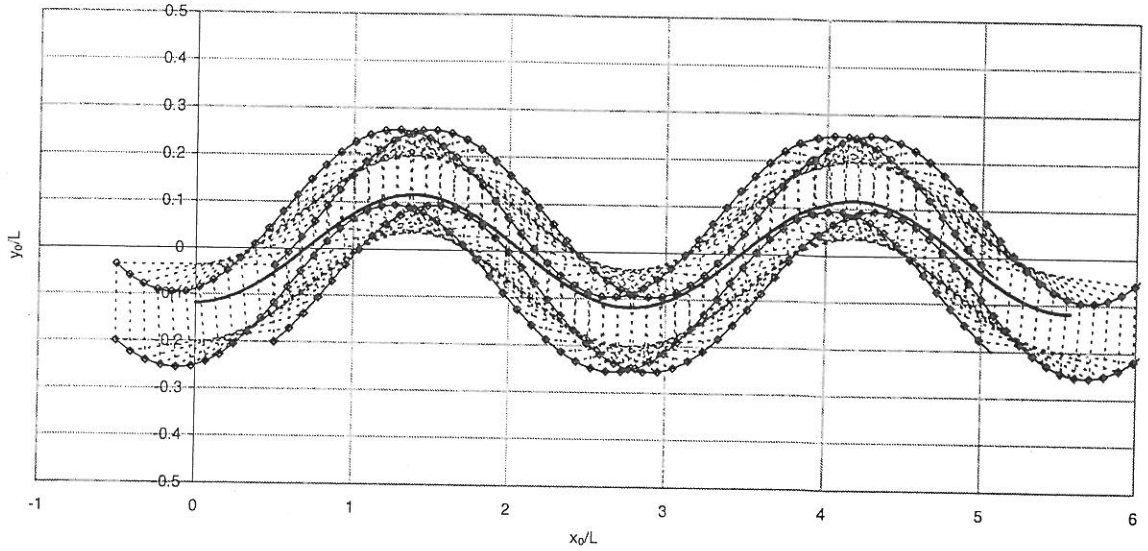

Figure 23. Swept path of a ship with B/L = 0.16 during a PMM yaw test with ω'=2.2, ψ_A = 15 deg.

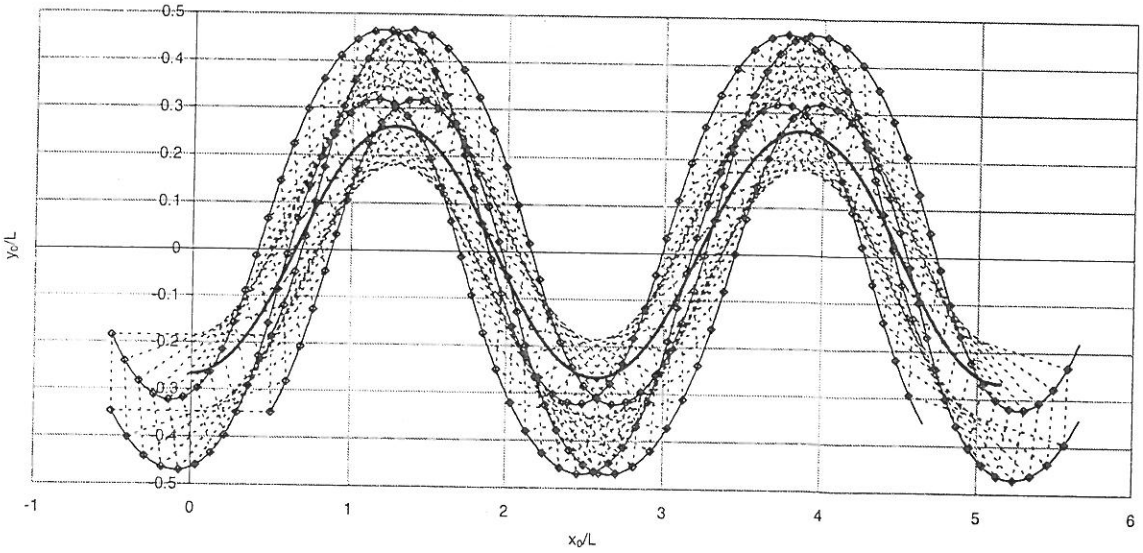

Figure 24. Swept path of a ship with B/L = 0.16 during a PMM yaw test with ω'=2.2, ψ_A = 35 deg.